ELSEVIER

International Journal of Solids and Structures 41 (2004) 3125–3150

INTERNATIONAL JOURNAL OF SOLIDS and STRUCTURES

www.elsevier.com/locate/ijsolstr

On modeling the deformation and fracture response of glassy polymers due to shear-yielding and crazing

B.P. Gearing, L. Anand *

Department of Mechanical Engineering, Massachusetts Institute of Technology, Room 1-310, Cambridge, MA 02139 4307, USA

Received 22 May 2003; received in revised form 8 December 2003

Available online 5 March 2004

Abstract

We have developed a constitutive model and failure criteria, which account for the competition between shear-yielding and crazing, and provide a framework for the quantitative prediction of the deformation and fracture response of glassy polymers. To represent shear-yielding we use the model of Boyce et al. (e.g. [Mech. Mater. 7 (1988) 15]), which has been recently re-formulated by Anand and Gurtin [Int. J. Solids Struct. 40 (2003) 1465]. To model crazing, we introduce a continuum constitutive relation which contains the three ingredients of crazing: initiation, widening, and breakdown. We allow for local inelastic deformation due to shear-yielding in possible concurrence with that due to crazing, and introduce a craze-initiation criterion based on the local maximum principal tensile stress reaching a critical value which depends on the local mean normal stress. After crazing has initiated, our continuum model represents the transition from shear-flow to craze-flow by a change in the viscoplastic flow rule, in which the dilational inelastic deformation associated with craze-plasticity is taken to occur in the direction of the local maximum principal stress. Finally, for situations in which the local maximum tensile stress is positive, craze-breakdown and fracture is taken to occur when a local tensile plastic craze strain reaches a critical value. We have implemented our constitutive model in a finite-element computer program. This finite-element program permits the modeling of failure by an element-removal technique.

We have calibrated the constitutive parameters in our model for the important glassy polymer, polymethylmethacrylate (PMMA) under normal dry conditions. We show that our model, when suitably calibrated and implemented, is able to reasonably-well predict the macroscopic load–displacement curves, and local aspects of the craze-flow and fracture processes in (a) a thin plate with a circular hole under tension, and (b) a notched beam in four-point bending.

Keywords: Polymeric material; Constitutive behavior; Fracture criteria; Mechanical testing; Finite elements

1. Introduction

Under stress states where the maximum principal stress is compressive, amorphous glassy polymers typically show extensive plastic deformation by a "shear yielding" mechanism which involves profuse

* Corresponding author. Tel.: +1-617-253-1635; fax: +1-617-258-8742.
E-mail address: anand@mit.edu (L. Anand).

0020-7683/$ - see front matter © 2004 Elsevier Ltd. All rights reserved.
doi:10.1016/j.ijsolstr.2004.01.017

densely-packed microscopic shear bands; the material shows substantial ductility, and eventual fracture occurs at large stretches by a chain-scission mechanism. In contrast, under stress states where the maximum principal stress is tensile, glassy polymers may at first show a little (or no) macroscopic inelastic deformation due to shear-yielding, but then the mechanism of inelastic deformation switches to "crazing". An individual craze is a thin plate-like microscopic region in the material with a microstructure distinguished by a dense array of fibrils (interspersed with elongated voids) which span the boundaries of the individual crazes. The plate boundaries of the crazes are typically oriented perpendicular to the maximum principal stress direction, and the dominant inelastic deformation occurs by craze widening in the local maximum principal stress direction. Macroscopically, however, the material shows little ductility, and the nominally brittle fracture occurs by craze-breakdown, crack-formation and crack-growth to failure. In most high molecular weight, flexible chain glassy polymers, such as polystyrene (PS) and polymethylmethacrylate (PMMA), [1] fracture under stress states where the maximum principal stress is tensile, is preceded by this craze-initiation, widening, and breakdown process (e.g. Kambour, 1973; Kramer, 1983).

A significant advance in modeling the plastic deformation of amorphous polymers by shear-yielding has been made by Parks et al. and their co-workers (e.g. Parks et al., 1985; Boyce et al., 1988; Arruda and Boyce, 1993), and by Wu and Van der Giessen (1993); more recently, Anand and Gurtin (2003) have reformulated the theory within a rigorous thermodynamic framework. In contrast, although the phenomenon of crazing has been widely studied over the past four decades, and considerable understanding of the micromechanisms of crazing and cracking in amorphous polymers has been developed (e.g. Kambour, 1973; Andrews, 1973; Argon and Hannoosh, 1977; Kramer, 1983; Narisawa and Yee, 1993; Donald, 1997), *the incorporation of this understanding into an engineering tool for the quantitative prediction of the deformation and fracture response of glassy polymers is just beginning to emerge* (e.g. Estevez et al., 2000; Tijssens et al., 2000a,b; Socrate et al., 2001).

Most studies on fracture of glassy polymers are based on the standard framework of linear elastic fracture mechanics (e.g. Kinloch and Young, 1983; Williams, 1984). However, as noted by Estevez et al. (2000), this approach ignores the process of initiation, widening and breakdown of crazes, and cannot be used when shear-yielding of the material may be occurring at other locations in the body, especially when there are no initial sharp cracks in the body. Classical fracture mechanics cannot deal with crack nucleation, and the numerical simulation of crack propagation has also been a challenge for this classical theory. The recent work of Van der Giessen and co-workers (e.g. Estevez et al., 2000; Tijssens et al., 2000a,b) and Socrate et al. (2001) is based on "cohesive surface" modeling of craze-initiation, growth and breakdown. [2] Cohesive surface modeling of fracture started more than 40 years ago with the work of Barenblatt (1959) and Dugdale (1960). In recent years, cohesive surface models have been widely used to numerically simulate fracture initiation and growth by the finite-element method (e.g. Xu and Needleman, 1994; Camacho and Ortiz, 1996). Typically, a set of cohesive surfaces are introduced in the finite-element discretization by the use of special interface elements which obey a non-linear interface traction-separation constitutive relation which provides a phenomenological description for the complex microscopic processes that lead to the formation of new traction-free crack faces. The loss of cohesion, and thus crack nucleation and extension occurs by the progressive decay of interface tractions. The interface traction-separation relation usually includes a cohesive strength and cohesive work-to-fracture. Once the local strength and work-to-fracture criteria across an interface are met, decohesion occurs naturally across the interface, and traction-free cracks form and propagate along element boundaries. An important characteristic of this methodology for modeling fracture initiation and propagation is that macroscopic fracture criteria, based on elastic or elastic–plastic analyses, such as $K_I = K_{IC}$ or $J_I = J_{IC}$, are not needed, because material strength and

[1] But not polycarbonate, which does not craze under normal circumstances in the absence of solvents.

[2] Socrate et al. (2001) do not consider the breakdown stage which leads to final fracture.

toughness, and crack nucleation and propagation are all characterized by the local traction-separation relation and the cohesive surface methodology. [3] Of special note is that the interface constitutive model used by Van der Giessen and co-workers (e.g. Estevez et al., 2000; Tijssens et al., 2000a,b) is an *elastic–viscoplastic traction-separation relation* which accounts for the three separate stages of craze-initiation, widening, and breakdown. While Van der Giessen and co-workers have produced informative *two-dimensional* parametric numerical studies on craze-initiation, crack formation and crack growth around circular holes in plates under far-field tension, and in cracked plates under mode I loading conditions, much work remains to be done to correlate their parametric studies with actual experimental results, and to develop a truly predictive numerical capability for engineering design.

The purpose of the present paper is to *present an alternative approach to modeling the competition between shear-yielding and crazing, and to develop the framework of an engineering tool for the quantitative prediction of the deformation and fracture response of glassy polymers*. Instead of attempting to represent each individual craze with an interface element, we will use a continuum constitutive relation which contains the three ingredients of crazing, viz., initiation, widening, and breakdown. Our model shall not account for the typical fine microstructural details of crazing; instead, for the continuum level of interest here, the inelastic deformation due to crazing will be defined as an average over a microstructural representative volume element that contains enough plate-like craze regions to result in an acceptably smooth process at the macroscopic level (prior to fracture). We will allow for local inelastic deformation due to shear-yielding in possible concurrence with that due to crazing, and introduce a simple craze-initiation criterion based on the local maximum principal tensile stress reaching a critical value which depends on the local mean normal stress. After crazing has initiated, our continuum model will represent the transition from shear-flow to craze-flow by a change in the viscoplastic flow rule, in which the dilational inelastic deformation associated with craze-plasticity will be taken to occur in the direction of the local maximum principal stress. [4] Finally, in order to model fracture we shall adopt a simple rule: for situations in which the local maximum tensile stress is positive, fracture will be taken to occur when a local tensile plastic craze strain reaches a critical value.

We have implemented our constitutive model in the finite-element computer program ABAQUS/Explicit ABAQUS (2002) by writing a user material subroutine. This finite-element program permits the modeling of failure, when user-specified critical values of certain parameters are reached, by an element-removal technique. By employing an appropriately dense (but computationally efficient) finite-element mesh, we shall show that it is possible to predict, with reasonable quantitative accuracy, the major features of the macroscopic deformation and fracture behavior of components made from glassy polymers which craze.

In particular, we shall demonstrate that our model, when suitably implemented and calibrated against a suite of experiments to determine the constitutive parameters in the model for PMMA, is able to reasonably-well predict the macroscopic load–displacement curves, and local aspects of the craze-flow and fracture processes in (a) a thin plate with a circular hole under tension, and (b) a notched beam in four-point bending, made from this important glassy polymer.

[3] There are still at least two key issues that need to be addressed in the cohesive surface modeling of fracture: (a) While it is relatively straightforward to construct a traction-separation relation for normal separation across an interface to model mode I conditions, elastic–plastic traction-separation relations for combined opening and sliding, together with the experimental methods needed to determine the parameters that might enter such coupled interface constitutive relations, are not well-developed, even for two-dimensional problems, and this issue is expected to be substantially more complicated in three dimensions. (b) The cohesive interface approach numerically restrains the orientation of crack nucleation and propagation. Once a finite-element mesh is chosen, the crack can only nucleate and grow along the element boundaries. In the case of crazing, the initial element boundaries may not be aligned perpendicular to the evolving local maximum principal stress direction.

[4] By incorporating such a constitutive model which allows for a local switch in the flow rule from shear-flow to craze-flow, we avoid a priori assumptions concerning the orientation and location of interface elements for crazing, assumptions which are inherent in the cohesive interface approach.

The plan of this paper is as follows. In Section 2 we develop our constitutive model. In Section 3 we describe our experiments to calibrate the material parameters in the model for PMMA; we limit our study to experiments performed under normal dry conditions. In Section 4 we verify the predictive capabilities of our constitutive model and computational procedures for the deformation and fracture response of notched components made from PMMA. We close in Section 5 with some final remarks.

2. Constitutive equations for plastic deformation. Fracture criteria

In this section we begin by summarizing the constitutive model for plastic deformation of amorphous polymeric materials by the shear-yielding mechanism that we shall use in this paper (Anand and Gurtin, 2003). This (isothermal) model is based on the multiplicative decomposition, $\mathbf{F} = \mathbf{F}^{\mathrm{e}}\mathbf{F}^{\mathrm{p}}$, of the deformation gradient $\mathbf{F}$ into elastic and plastic parts, $\mathbf{F}^{\mathrm{e}}$ and $\mathbf{F}^{\mathrm{p}}$ (Kroner, 1960; Lee, 1969). [5] The model also contains two internal variables: a variable $s > 0$ that represents an isotropic intermolecular resistance to plastic flow; and an unsigned variable η that represents the local free-volume. [6] Then, in terms of the variables

ψ Helmholtz free energy per unit volume of the relaxed configuration
$\mathbf{T}$, $\mathbf{T} = \mathbf{T}^{\top}$ Cauchy stress
$\mathbf{F}$, $\det\mathbf{F} > 0$ deformation gradient
$\mathbf{F}^{\mathrm{p}}$, $\det\mathbf{F}^{\mathrm{p}} = 1$ plastic part of the deformation gradient
s, $s > 0$ isotropic resistance to plastic flow
η free-volume

and the definitions

$\mathbf{F}^{\mathrm{e}} = \mathbf{F}\mathbf{F}^{\mathrm{p}^{-1}}$, $\det\mathbf{F}^{\mathrm{e}} > 0$ elastic deformation gradient
$\mathbf{C}^{\mathrm{e}} = \mathbf{F}^{\mathrm{e}^{\top}}\mathbf{F}^{\mathrm{e}}$ elastic right Cauchy–Green strain
$\mathbf{E}^{\mathrm{e}} = \frac{1}{2}(\mathbf{C}^{\mathrm{e}} - 1)$ elastic strain
$\mathbf{T}^{\mathrm{e}} = \mathbf{R}^{\mathrm{e}^{\top}}\mathbf{T}\mathbf{R}^{\mathrm{e}}$ stress conjugate to the elastic strain $\mathbf{E}^{\mathrm{e}}$
$\sigma = \frac{1}{3}\mathrm{tr}\,\mathbf{T}$ mean normal stress
$\mathbf{T}^{\mathrm{e}}_0 = \mathbf{T}^{\mathrm{e}} - \sigma\mathbf{1}$ deviatoric stress
$\mathbf{T}^{\mathrm{e}} = \sum_{i=1}^{3}\sigma_i\mathbf{e}_i \otimes \mathbf{e}_i$, with $\sigma_1 \geqslant \sigma_2 \geqslant \sigma_3$ spectral decomposition of $\mathbf{T}^{\mathrm{e}}$
$\mathbf{B}^{\mathrm{p}} = \mathbf{F}^{\mathrm{p}}\mathbf{F}^{\mathrm{p}^{\top}}$ left Cauchy–Green tensor corresponding to $\mathbf{F}^{\mathrm{p}}$
$\mathbf{B}^{\mathrm{p}}_0 = \mathbf{B}^{\mathrm{p}} - \frac{1}{3}(\mathrm{tr}\,\mathbf{B}^{\mathrm{p}})\mathbf{1}$ deviatoric part of $\mathbf{B}^{\mathrm{p}}$
$\lambda^{\mathrm{p}} = \frac{1}{\sqrt{3}}\sqrt{\mathrm{tr}\,\mathbf{B}^{\mathrm{p}}}$ effective distortional plastic stretch
$\mathbf{D}^{\mathrm{p}} = \mathrm{sym}(\dot{\mathbf{F}}^{\mathrm{p}}\mathbf{F}^{\mathrm{p}^{-1}})$, $\mathrm{tr}\,\mathbf{D}^{\mathrm{p}} = 0$ plastic stretching

the constitutive equations, under the approximative assumption of small elastic stretches, are:

[5] *Notation*: ∇ and Div denote the gradient and divergence with respect to the material point $\mathbf{X}$ in the *reference configuration*; grad and div denote these operators with respect to the point $\mathbf{x} = \mathbf{y}(\mathbf{X}, t)$ in the deformed configuration, where $\mathbf{y}(\mathbf{X}, t)$ is the motion; a superposed dot denotes the material time-derivative. The deformation gradient, velocity and velocity gradient are given by $\mathbf{F} = \nabla\mathbf{y}$, $\mathbf{v} = \dot{\mathbf{y}}$, and $\mathbf{L} = \mathrm{grad}\,\mathbf{v} = \dot{\mathbf{F}}\mathbf{F}^{-1}$, respectively. Throughout, we write $\mathbf{F}^{\mathrm{e}^{-1}} = (\mathbf{F}^{\mathrm{e}})^{-1}$, $\mathbf{F}^{\mathrm{p}^{-\top}} = (\mathbf{F}^{\mathrm{p}})^{-\top}$, etc. We write $\mathrm{aym}\,\mathbf{A}$, $\mathrm{skw}\,\mathbf{A}$, respectively, for the symmetric, and skew parts of a tensor $\mathbf{A}$. The deviatoric part of a tensor $\mathbf{A}$ is denoted by $\mathbf{A}_0$. Also, the inner product of tensors $\mathbf{A}$ and $\mathbf{B}$ is denoted by $\mathbf{A}\cdot\mathbf{B}$, and the magnitude of $\mathbf{A}$ by $|\mathbf{A}| = \sqrt{\mathbf{A}\cdot\mathbf{A}}$.

[6] It is commonly believed that the evolution of the local free-volume is the major reason for the highly non-linear stress–strain behavior of glassy materials which precedes the yield-peak and gives rise to the post-yield strain-softening.

(1) *Free energy*

The Helmholtz free energy is taken in the non-interactive form

$$\psi = \psi^{\mathrm{e}}(\mathbf{E}^{\mathrm{e}}) + \psi^{\mathrm{p}}(\lambda^{\mathrm{p}}), \tag{2.1}$$

where ψ^{e} is an elastic free energy, and ψ^{p} a plastic free energy. The elastic free energy is taken in the standard form for small elastic stretches

$$\psi^{\mathrm{e}} = G|\mathbf{E}^{\mathrm{e}}_0|^2 + \frac{1}{2}K|\mathrm{tr}\,\mathbf{E}^{\mathrm{e}}|^2, \tag{2.2}$$

where G and K are the elastic shear and bulk moduli, respectively. In amorphous polymeric materials the major part of ψ^{p} arises from an "entropic" contribution, and motivated by statistical mechanics models of rubber elasticity, [7] is taken in the specific form

$$\psi^{\mathrm{p}} = \mu_R \lambda_L^2 \left[\left(\frac{\lambda^{\mathrm{p}}}{\lambda_L} \right) x + \ln\left(\frac{x}{\sinh x} \right) - \left(\frac{1}{\lambda_L} \right) y - \ln\left(\frac{y}{\sinh y} \right) \right], \tag{2.3}$$

$$x = \mathscr{L}^{-1}\left(\frac{\lambda^{\mathrm{p}}}{\lambda_L} \right), \quad y = \mathscr{L}^{-1}\left(\frac{1}{\lambda_L} \right), \tag{2.4}$$

where $\mathscr{L}^{-1}$ is the inverse [8] of the Langevin function $\mathscr{L}(\cdots) = \coth(\cdots) - (\cdots)^{-1}$. This functional form for ψ^{p} involves two material parameters: μ_R, called the rubbery modulus, and λ_L called the network locking stretch.

(2) *Equation for the stress*

$$\mathbf{T}^{\mathrm{e}} = \frac{\partial \psi^{\mathrm{e}}}{\partial \mathbf{E}^{\mathrm{e}}} = 2G\mathbf{E}^{\mathrm{e}}_0 + K(\mathrm{tr}\,\mathbf{E}^{\mathrm{e}})\mathbf{1}. \tag{2.5}$$

(3) *Equation for back stress* [9]

$$\mathbf{S}_{\mathrm{back}} = 2\mathrm{sym}_0\left(\frac{\partial \psi^{\mathrm{p}}}{\partial \mathbf{B}^{\mathrm{p}}} \mathbf{B}^{\mathrm{p}} \right) = \mu \mathbf{B}^{\mathrm{p}}_0, \quad \text{with} \tag{2.6}$$

$$\mu = \frac{1}{3\lambda^{\mathrm{p}}} \frac{\partial \psi^{\mathrm{p}}}{\partial \lambda^{\mathrm{p}}} = \mu_R \left(\frac{\lambda_L}{3\lambda^{\mathrm{p}}} \right) \mathscr{L}^{-1}\left(\frac{\lambda^{\mathrm{p}}}{\lambda_L} \right). \tag{2.7}$$

The back stress modulus $\mu \to \infty$ as $\lambda^{\mathrm{p}} \to \lambda_L$, since $\mathscr{L}^{-1}(z) \to \infty$ as $z \to 1$.

(4) *Flow rule*

The evolution equation for $\mathbf{F}^{\mathrm{p}}$ is

$$\dot{\mathbf{F}}^{\mathrm{p}} = \mathbf{D}^{\mathrm{p}}\mathbf{F}^{\mathrm{p}}, \quad \mathbf{F}^{\mathrm{p}}(\mathbf{X}, 0) = \mathbf{1}, \tag{2.8}$$

with $\mathbf{D}^{\mathrm{p}}$ given by the flow rule

$$\mathbf{D}^{\mathrm{p}} = \nu^{\mathrm{p}} \left(\frac{\mathbf{T}^{\mathrm{e}}_0 - \mathbf{S}_{\mathrm{back}}}{2\bar{\tau}} \right), \quad \nu^{\mathrm{p}} = \nu_0 \left(\frac{\bar{\tau}}{s - \alpha\sigma} \right)^{\frac{1}{m}}, \quad 0 < m \leqslant 1, \tag{2.9}$$

[7] Cf., Treloar (1975), Arruda and Boyce (1993), Anand (1996).

[8] To evaluate $x = \mathscr{L}^{-1}(y)$ for a given y in the range $0 < y < 1$, we numerically solve the non-linear equation $f(x) = \mathscr{L}(x) - y = 0$ for x.

[9] Also see Arruda and Boyce (1993).

where

$$\bar{\tau} = \frac{1}{\sqrt{2}}|\mathbf{T}_0^{\mathrm{e}} - \mathbf{S}_{\mathrm{back}}|, \quad \text{and} \quad v^{\mathrm{p}} = \sqrt{2}|\mathbf{D}^{\mathrm{p}}|, \tag{2.10}$$

are an equivalent shear stress and equivalent plastic shear-strain rate, respectively. Here, v_0 is a reference plastic shear-strain rate, α a pressure sensitivity parameter, and m a strain-rate sensitivity parameter. The limit $m \to 0$ renders (2.9) rate-independent, while $m = 1$ renders (2.9) linearly viscous.

(5) *Evolution equations for the internal variables s and η*

A key feature controlling the initial plastic deformation of amorphous materials is the evolution of the local free-volume associated with the metastable state of these materials, and it is commonly believed that for glassy polymers the evolution of this free-volume is the major reason for the highly non-linear stress–strain behavior that precedes the yield-peak and gives rise to post-yield strain-softening. During this initial stage of the loading process we expect the free-volume η to increase monotonically to an equilibrium value η_{cv}. On the other hand, the observed yield-peak suggests that the flow resistance s first increases smoothly to a peak value and then decrease smoothly to an equilibrium value s_{cv}. With this in mind, the evolution of s and η are taken to be governed by the coupled differential equations [10]

$$\left.\begin{aligned} \dot{s} &= h_0\left(1 - \tfrac{s}{\tilde{s}(\eta)}\right)v^{\mathrm{p}}, \quad s(\mathbf{X},0) = s_0, \\ \dot{\eta} &= g_0\left(\tfrac{s}{s_{\mathrm{cv}}} - 1\right)v^{\mathrm{p}}, \quad \eta(\mathbf{X},0) = 0, \end{aligned}\right\} \tag{2.11}$$

with

$$\tilde{s}(\eta) = s_{\mathrm{cv}}[1 + b(\eta_{\mathrm{cv}} - \eta)], \tag{2.12}$$

where $\{h_0, g_0, s_{\mathrm{cv}}, b, \eta_{\mathrm{cv}}\}$ are additional material parameters. Here $\tilde{s} = \tilde{s}(\eta)$ is a saturation value of s: $\dot{s}$ is positive for $s < \tilde{s}$ and negative for $s > \tilde{s}$. By definition v^{p} is non-negative. Assuming that $v^{\mathrm{p}} > 0$, all solutions to the pair of evolution equations satisfy

$$s \to s_{\mathrm{cv}} \quad \text{and} \quad \eta \to \eta_{\mathrm{cv}} \quad \text{as } t \to \infty.$$

We restrict attention to the initial conditions $s = s_0$ with

$$s_0 \leqslant s \leqslant s_{\mathrm{cv}}(1 + b\eta_{\mathrm{cv}}).$$

Also, as is tacit from $(2.11)_2$, the free-volume is measured from the value $\eta = 0$ in the virgin state of the material, and thus η at any other time represents a change in the free-volume from the initial state.

2.1. Modification of the constitutive equations to model craze-initiation, flow, and breakdown

The overall inelastic deformation due to craze-initiation and growth is always inhomogeneous at the microstructural length scales associated with crazing. We emphasize that our model shall not account for the typical fine microstructural details of crazing. The spatially continuous fields that define our theory are to be considered as averages meant to apply at length scales which are large compared to those associated with the fine structure of the crazes and their distribution in a representative volume element. That is, for the continuum level of interest here, the inelastic deformation due to crazing will be defined as an average over a microstructural representative volume element (the material neighborhood of a continuum material point **X**) that contains enough plate-like craze regions to result in an acceptably smooth process.

What constitutes an appropriate model for craze-initiation is probably the least well-agreed-upon ingredient of the overall modeling of crazing in the literature. Argon and coworkers (e.g. Argon and

[10] We expect that $\tilde{s}$ (and perhaps h_0 and g_0) may, in general, depend on v^{p}, but currently there is insufficient experimental evidence to warrant such a refinement.

Hannoosh, 1977; Argon et al., 1977) have emphasized that stress-based criteria governing initiation are hard to determine with precision from experiments because of the importance of imperfections in controlling the local stress states and the sites of craze-initiation. In tension–torsion, stress-controlled experiments on thin-walled tubular specimens with controlled microroughness, these authors observed that at stress levels where the equivalent shear stress, $\bar{\tau} = \sqrt{(1/2)\mathbf{T}_0 \cdot \mathbf{T}_0}$, and mean normal stress, σ, were below ≈ 0.5 of the yield strength Y of the material (due to shear-yielding), there was a time delay between the application of stress, and the first appearance of crazing. Their experiments showed that the delay time for craze-initiation decreases with increasing values of equivalent shear stress or mean normal stress, and becomes negligible at stress levels greater than ≈ 0.5 of the yield strength of the material. Under these circumstances, craze-initiation may be considered an instantaneous event when a suitable local critical stress state is reached. Since we are concerned with the competition between shear-yielding and crazing, and eventually craze-breakdown and fracture, which typically occurs at stress levels higher than ≈ 0.5 of the yield strength, *we will ignore considerations of incubation times, and adopt a simple time-independent stress-based criterion for craze-initiation*. In this time-independent limit, Argon and Hannoosh (1977) have suggested that under situations in which the local mean normal stress is positive, $\sigma > 0$, crazes initiate when the local equivalent shear stress reaches a mean normal stress-dependent critical value (their Eq. (22)):

$$\bar{\tau} = \bar{\tau}_{\rm cr}(\sigma) > 0, \quad \text{with } \bar{\tau}_{\rm cr}(\sigma) = \frac{AY}{C + 3\sigma/2YQ}. \tag{2.13}$$

Here $Q = 0.0133$ is a fixed factor controlling the dependence $\bar{\tau}_{\rm cr}$ on the mean normal stress σ, and (A, C) are temperature-dependent material constants. Although, Argon and co-workers have suggested (2.13) as the time-independent limiting form of their detailed micromechanical time-dependent model, [11] this criterion does not reveal that at an instant when crazes might be considered to have initiated in a *macroscopic sense*, they are typically oriented perpendicular to the maximum principal tensile stress direction.

The earliest stress-based craze-initiation criterion is due to Sternstein and co-workers (e.g. Sternstein and Ongchin, 1969; Sternstein and Meyers, 1973). Based on biaxial plane-stress ($\sigma_3 = 0$) experiments on PMMA plates with circular holes, they postulated that the critical condition for craze nucleation is when a "stress bias" σ_B reaches a critical value

$$\sigma_B = \frac{A}{\sigma} + B, \tag{2.14}$$

where A and B are temperature-dependent material parameters. Under plane stress conditions with $\sigma_3 = 0$, they defined the stress bias by $\sigma_B = |\sigma_1 - \sigma_2|$. This quantity is the difference between the maximum and intermediate principal stresses when σ_1 and σ_2 are positive; however, it becomes the difference between the maximum and the minimum principal stress when either σ_1 or σ_2 is compressive. Thus, as noted by Oxborough and Bowden (1973), the physical interpretation of σ_B is unclear, nor is it clear how to evaluate σ_B for a general triaxial stress state. A further difficulty with this criterion is that while $|\sigma_1 - \sigma_2|$ represents an in-plane shear stress intensity, the crazes actually nucleate and grow in the direction of the maximum principal tensile stress. Noting this difficulty, Oxborough and Bowden (1973), based on their own experiments on PS, found that their experimental data for craze-initiation was better fit to a criterion in which the maximum principal tensile strain ϵ_1 reaches a critical value which depends on the mean normal stress σ:

[11] They modeled craze-initiation by postulating: (i) the formation of microcavities by the arrest of intense localized plastic flow at a molecular scale, with the rate at which such microcavities form depending on the local equivalent shear stress; (ii) the growth of these microcavities by plastic expansion into spongy craze nuclei, with the rate at which the microcavities grow depending on the local equivalent shear stress and the mean normal stress; (iii) the subsequent growth of the spongy craze nucleus by a meniscus instability mechanism, to initiate a macroscopic craze. Based on this micromechanical model they developed an expression which provides an estimate for the time to initiate a craze under a given stress state.

$$\epsilon_1 = \epsilon_{1,\mathrm{cr}}(\sigma) > 0, \quad \text{with } \epsilon_{1,\mathrm{cr}} = \frac{X'}{\sigma} + Y', \tag{2.15}$$

where X' and Y' are temperature-dependent parameters. Since $\epsilon_1 = \{\sigma_1 - \nu(\sigma_2 + \sigma_3)\}/E$ for an isotropic elastic material, with (E, ν) the usual Young's modulus and Poisson's ratio, this criterion may be written as

$$\sigma_1 - \nu(\sigma_2 + \sigma_3) = \frac{X}{\sigma} + Y, \tag{2.16}$$

where $X = EX'$ and $Y = EY'$. For plane stress this equation is very similar to the criterion (2.14) proposed by Sternstein and Ongchin (1969).

The craze-initiation criterion (2.16) of Oxborough and Bowden may be further rearranged as a criterion in stress space, wherein craze-initiation may be taken to occur when the maximum principal stress σ_1 reaches a critical value which depends on the mean normal stress σ:

$$\sigma_1 = \sigma_{1,\mathrm{cr}}(\sigma) > 0, \quad \text{with } \sigma_{1,\mathrm{cr}}(\sigma) = c_1 + \frac{c_2}{\sigma} + c_3\sigma, \tag{2.17}$$

where $c_1 = Y/(1+\nu)$, $c_2 = X/(1+\nu)$, and $c_3 = 3\nu/(1+\nu)$.

Based on this brief review of the literature, in this paper we shall assume that crazing in a representative volume element (the material neighborhood of a continuum material point **X**) can *initiate* provided the following two conditions are met:

(C1) the maximum principal stress and the mean normal stress are positive

$$\sigma_1 > 0, \quad \sigma = \frac{1}{3}(\sigma_1 + \sigma_2 + \sigma_3) > 0; \tag{2.18}$$

and

(C2) the maximum principal stress σ_1 reaches a mean normal stress-dependent critical value

$$\sigma_1 = \sigma_{1,\mathrm{cr}}(\sigma) > 0. \tag{2.19}$$

After crazing has initiated and has become fully-developed, the average macroscopic plastic flow becomes oriented in the direction of the maximum principal stress. The dominant inelastic deformation associated with fully-developed craze-plasticity occurs by widening of the crazes in the direction of the maximum principal stress. Following Argon (1999), the macroscopic averaged tensile plastic strain rate ξ^{p} may be kinematically related to the lateral translation of a given volume fraction of active craze borders as depicted schematically in Fig. 1, which shows active planar crazes separated by an average spacing h, thickening at an average rate $\dot{\delta}$, such that $\xi^{\mathrm{p}} = \dot{\delta}/h$.

In our continuum model we will represent the transition from shear-flow to craze-flow by a change in the flow rule. To do this we use a switching parameter χ having values

$$\chi = \begin{cases} 1 & \text{if conditions C1 and C2 are met,} \\ 0 & \text{otherwise.} \end{cases} \tag{2.20}$$

Once the craze-initiation conditions C1 and C2 have been met, the craze-flow will be taken to continue as long as the maximum principal stress is positive. Accordingly, we set

$$\mathbf{D}^{\mathrm{p}} = \begin{cases} \nu^{\mathrm{p}}\left(\frac{\mathbf{T}_0^{\mathrm{e}} - \mathbf{S}_{\mathrm{back}}}{2\bar{\tau}}\right), & \nu^{\mathrm{p}} = \nu_0\left(\frac{\bar{\tau}}{s - \alpha\sigma}\right)^{\frac{1}{m}}, \quad \text{if } \chi = 0, \\ \xi^{\mathrm{p}}\hat{\mathbf{e}}_1 \otimes \hat{\mathbf{e}}_1, & \xi^{\mathrm{p}} = \xi_0\left\{\frac{\sigma_1}{s_{\mathrm{craze}}}\right\}^{\frac{1}{m}}, \quad \text{if } \chi = 1 \text{ and } \sigma_1 > 0. \end{cases} \tag{2.21}$$

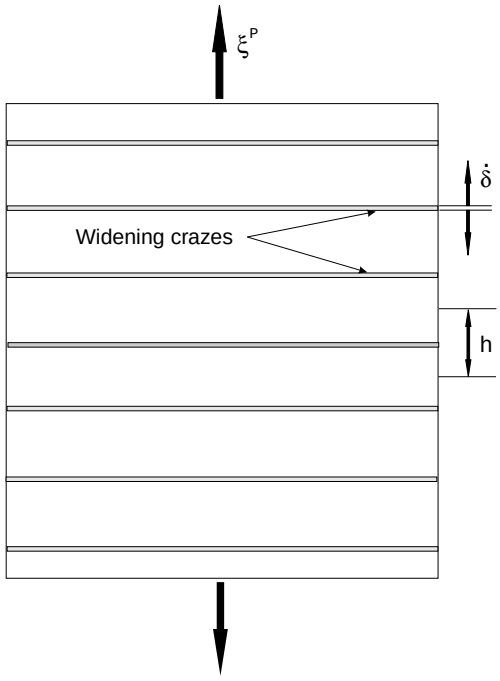

Fig. 1. An idealization of craze-plasticity where the macroscopic averaged tensile craze strain rate ξ^{p} is determined by the thickening rate $\dot{\delta}$ of crazes at an average spacing h. After Argon (1999), Fig. 7.

Here, ξ_0 is a reference craze strain rate, and s_{craze} is the resistance to craze-flow, which we take to be a constant. Also, m is the strain-rate sensitivity parameter for craze-flow, which is taken to be the same as that for shear-flow. We call

$$\epsilon^{\mathrm{p}} = \int \xi^{\mathrm{p}} \, \mathrm{d}t \tag{2.22}$$

the *craze-strain*.

Finally, in order to model craze-breakdown and fracture, we adopt the simple rule that for situations in which $\sigma_1 > 0$, craze-breakdown occurs when the local craze-strain ϵ^{p} reaches a failure value $\epsilon^{\mathrm{p}}_{\mathrm{f}}$:

$$\epsilon^{\mathrm{p}} \leqslant \epsilon^{\mathrm{p}}_{\mathrm{f}}. \tag{2.23}$$

On the other hand, for situations when $\sigma_1 \leqslant 0$, ductile fracture due to molecular chain-scission will be taken to initiate when the effective plastic stretch, λ^{p}, reaches a critical value $\lambda^{\mathrm{p}}_{\mathrm{f}}$:

$$\lambda^{\mathrm{p}} \leqslant \lambda^{\mathrm{p}}_{\mathrm{f}}. \tag{2.24}$$

We have implemented our constitutive model in the finite-element computer program ABAQUS/Explicit ABAQUS (2002) by writing a user material subroutine. This finite-element program permits the modeling of failure, by an element-removal technique. To avoid numerical instabilities, once either of the two fracture criteria are met, the corresponding material resistances are not instantly set to zero, but rapidly decreased to zero within a few increments. [12]

[12] We recognize that our element-removal methodology implicitly introduces an unspecified small time-constant during which the stresses decay to zero. A better, more formal approach would be to incorporate a damage variable, whose evolution reduces the effective moduli, creating a stable fracture mechanism that couples the fracture in a continuous sense to the already formulated features of the model. We leave such a refinement for future work.

3. Estimation of material parameters for PMMA

In this section we present the results of our efforts at estimation of the material parameters for our constitutive model, and also the failure values of the craze-strain and the effective plastic stretch, in the fracture criteria. Recall that the material parameters that need to be determined are

(1) The elastic shear and bulk moduli (G, K) in the elastic part of the free energy.
(2) The parameters (μ_R, λ_L) in the plastic part of the free energy.
(3) The parameters $\{v_0, m, \alpha, h_0, g_0, s_{\rm cv}, b, \eta_{\rm cv}, s_0\}$ in the flow rule and the evolution equations for (s, η) for shear-flow.
(4) The function $\sigma_{1,\rm cr}(\sigma)$ in the craze-initiation criterion, and the parameters $\{\xi_0, s_{\rm craze}, m\}$ in the function for craze-flow.
(5) The parameters $\{\epsilon_{\rm f}^{\rm p}, \lambda_{\rm f}^{\rm p}\}$ in the failure criteria.

The values of elastic moduli (G, K) are determined by measuring the Young's modulus E and Poisson's ratio ν of the material in a compression experiment and using standard conversion relations of isotropic elasticity to obtain the elastic shear and bulk moduli. The parameters $\{v_0, m\}$ are estimated by conducting a strain-rate jump experiment in simple compression. The pressure sensitivity parameter α is estimated from compression experiments under superposed hydrostatic pressure reported in the literature. The remaining parameters $\{h_0, g_0, s_{\rm cv}, b, \eta_{\rm cv}, s_0\}$ and (μ_R, λ_L) for shear-flow may be estimated by fitting a stress–strain curve in compression to large strains.

The craze-initiation function $\sigma_{1,\rm cr}(\sigma)$ is estimated from three sets of experiments: (a) smooth-bar tension tests, (b) notched-bar tension tests, and (c) tests on compact tension specimens (CTS) which contain the standard notch geometry, but are not fatigue pre-cracked. These three sets of experiments are chosen to provide a reasonably large range of positive mean normal stresses, σ, at craze-initiation.

For the craze-flow parameters, $\{\xi_0, s_{\rm craze}, m\}$, the strain-rate sensitivity m is taken to be the same as that for shear-flow; the parameter $s_{\rm craze}$ which represents the craze-matter resistance to stretching is estimated from the stress levels observed in the simple compression experiment at large values of compression. The parameter ξ_0 is chosen to ensure continuity of the magnitude of the plastic stretching $|\mathbf{D}^{\rm p}|$ at the transition from shear-flow to craze-flow, this gives

$$\xi_0 = \left(\frac{v_0}{\sqrt{2}}\right)\left\{\left(\frac{s_{\rm craze}}{(s^* - \alpha\sigma^*)}\right)\left(\frac{\bar{\tau}^*}{\sigma_1^*}\right)\right\}^{\frac{1}{m}}, \tag{3.1}$$

where a quantity with a superscript (*) denotes the value of the quantity at the instant $\chi = 1$ when the change in the flow rule is triggered. The craze-breakdown parameter $\epsilon_{\rm f}^{\rm p}$ is estimated from the experiments on the notched compact-tension specimens.

Finally, since crazing is suppressed in plane strain compression, the parameter $\lambda_{\rm f}^{\rm p}$ for ductile failure is obtained by fitting a load–displacement curve obtained from a specimen which has been loaded to failure initiation in a plane strain compression experiment.

A stress–strain curve for PMMA obtained from a monotonic simple compression experiment conducted at a constant logarithmic strain rate of -0.001/s is shown in Fig. 2; absolute values of stress and strain are plotted. [13] After an initial approximately linear region, the stress–strain curve becomes markedly non-linear

[13] As is well known, the mechanical response of amorphous thermoplastics is very sensitive to prior thermomechanical processing history. All experiments reported in this paper were conducted on PMMA specimens which were annealed at the glass transition temperature of this material, 105 °C, for 2 h, and then furnace-cooled to room temperature in approximately 15 h. The experiments reported here were conducted under isothermal conditions at room temperature.

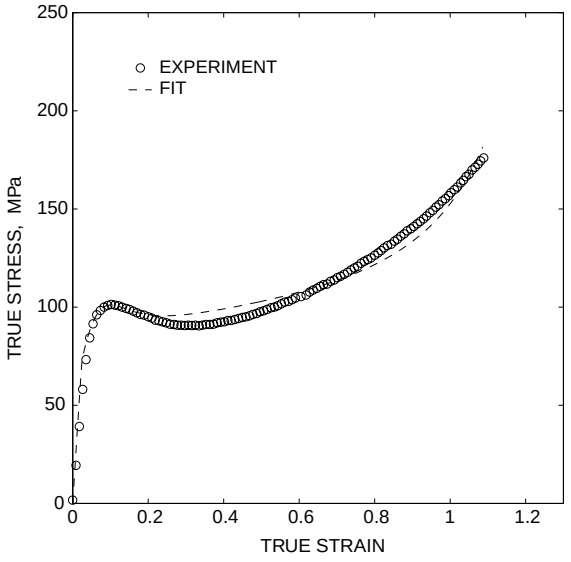

Fig. 2. Fit of the constitutive model to the stress–strain response of PMMA in simple compression.

prior to reaching a peak in the stress; the material then strain-softens to a quasi-plateau before beginning a broad region of rapid strain hardening. Using a value of $\alpha = 0.204$ (Rabinowitz et al., 1970), a value of $v_0 = 0.0017\ \text{s}^{-1}$ and a strain-rate sensitivity parameter $m = 0.043$ obtained from a strain-rate jump experiment, the parameters $\{G, K, \mu_R, \lambda_L, h_0, g_0, s_{\text{cv}}, b, \eta_{\text{cv}}, s_0\}$ were estimated by fitting the stress–strain curve for PMMA in simple compression, Fig. 2. [14] The fit was performed by judiciously adjusting the values of these parameters in finite-element simulations of a simple compression experiment (assuming homogeneous deformation) using a single ABAQUS/C3D8R element. After a few attempts, a reasonable fit was obtained, and the resulting stress–strain curve is shown in Fig. 2. The list of parameters obtained using this heuristic calibration procedure are: [15]

$$
\begin{aligned}
&G = 1.17\ \text{GPa} \quad K = 3.04\ \text{GPa} \quad \mu_R = 7.70\ \text{MPa} \quad \lambda_L = 1.51,\\
&v_0 = 0.0017\ \text{s}^{-1} \quad m = 0.043 \quad \alpha = 0.204,\\
&s_0 = 37.8\ \text{MPa} \quad s_{\text{cv}} = 43.7\ \text{MPa} \quad h_0 = 1.30\ \text{GPa},\\
&b = 790 \quad g_0 = 7.5 \cdot 10^{-3} \quad \eta_{\text{cv}} = 0.00025.
\end{aligned}
$$

Material parameters for craze-initiation, craze-flow, and craze-breakdown are estimated from suitable experiments and corresponding numerical simulations using the following three-step process:

[14] In fact, in determining G and K, we estimated the Young's modulus E form the stress–strain curve, and a literature value of Poisson's ratio of 0.33 for PMMA was assumed.

[15] This list, although not unique, is adequate for present purposes. We note that in addition to G, and K the parameters s_0, μ_R, and λ_L are *essential* to describe the plastic-locking response of the material. The only complexity in describing the shear-yielding response arises form the coupled differential equations for s and η, which require the set of material parameters $(h_0, g_0, s_{\text{cv}}, b, \eta_{\text{cv}}, s_0)$. If, for engineering purposes, the initial non-linearity in stress–strain curve and the gradual yield-peak, that is the "yield-transient", is not of sufficient interest, then the parameters $(h_0, g_0, s_{\text{cv}}, b, \eta_{\text{cv}})$ are not needed, and the task of material parameter determination becomes less onerous.

Step 1. First, the craze-initiation function $\sigma_{1,\mathrm{cr}}(\sigma)$ is estimated from three sets of experiments and corresponding numerical simulations: (a) Simple tension tests on smooth-bar specimens, which have an initial gauge section 6.35 mm in diameter and 25.4 mm in length, performed under displacement control at 0.0125 mm/s. (b) Notched-bar tension tests on 12.7 mm diameter cylindrical specimens with a notch of root-radius 0.90 mm, depth 3.18 mm, and width 1.80 mm. An extensometer was used to measure the local relative displacement across the notch faces as the specimen was extended at a rate of 0.0125 mm/s. (c) Tests on ASTM standard compact tension specimens (CTS) which contain a 60° notch, but are *not fatigue pre-cracked*. The compact tension specimens were tested at a displacement rate of 0.0125 mm/s. These three sets of experiments were chosen to provide a reasonably large range of positive mean normal stresses, σ, at craze-initiation. In our study, which is intended for *engineering applications*, we did not attempt to specially polish our specimens, but *used as-machined surfaces*. [16]

To check the repeatability of the response of the smooth-bar tension specimens, four identical specimens were tested. A representative load–displacement curve is shown in Fig. 3a; for this specimen, fracture occurs abruptly at a displacement of 1.64 mm. The measured displacements at fracture between the four experiments varied by less than 8%. All the smooth-bar specimens failed in the gauge section, some at multiple locations, and the fracture surface was always perpendicular to the tension direction. *The PMMA tension specimens show non-linearity prior to failure. This indicates that the material has undergone some shear-yielding prior to craze-flow and fracture.*

The repeatability of the response of the notched-bar tension experiments was investigated by conducting four experiments on nominally identical specimens. A representative experimental load–displacement curve is shown in Fig. 3b; for this specimen, fracture is seen to abruptly occur at a displacement of only 0.078 mm. The displacement at fracture varied by less than 7% between the four specimens that were tested.

A representative load–displacement response from the compact tension experiments is shown in Fig. 3c. The repeatability of the peak load between the four specimens was found to be within 2%. In these specimens, crazing initiated at the notch root, and subsequently a front of a *craze process zone* propagated in a *stable manner* into the specimen. The initiation of crazing occurs at a displacement of approximately 0.47 mm, and the load asymptotically falls to about zero load after a displacement of 1.2 mm.

To numerically model the smooth-bar tension and the notched-bar tension experiments, one-half of the respective specimens were meshed with 390 ABAQUS/CAX4R axisymmetric elements, and to model the CTS experiment, one half of the specimen was meshed using 5278 plane strain ABAQUS/CPE4R, with a very fine mesh density in the vicinity of the specimen mid-plane. To estimate the craze-initiation parameters, the shear-flow parameters for PMMA were used in the numerical simulations, but *craze-flow and craze-breakdown were numerically suppressed.* These numerical simulations provide estimates of $\sigma_{1,\mathrm{cr}}$ and σ at craze-initiation, which is taken to occur just prior to the peak loads observed in the experiments. The values estimated for smooth-bar tension are $\sigma_{1,\mathrm{cr}} = 76.0$ MPa, at $\sigma = 25.3$ MPa; for notched-bar tension $\sigma_{1,\mathrm{cr}} = 68.9$ MPa at $\sigma = 32.8$ MPa; and for the compact tension specimen $\sigma_{1,\mathrm{cr}} = 65.2$ MPa at $\sigma = 44.9$ MPa. The three data points are plotted in Fig. 4; estimated error bars associated with each data point are also given. The data is reasonably-well fit by the function

$$\sigma_{1,\mathrm{cr}}(\sigma) = c_1 + \frac{c_2}{\sigma} \tag{3.2}$$

with

$$c_1 = 45.60 \text{ MPa}, \quad c_2 = 785.56 \text{ MPa}^2.$$

[16] Typical surface roughness values for our specimens, resulting from the machining procedures used, are on the order of 1–10 μm.

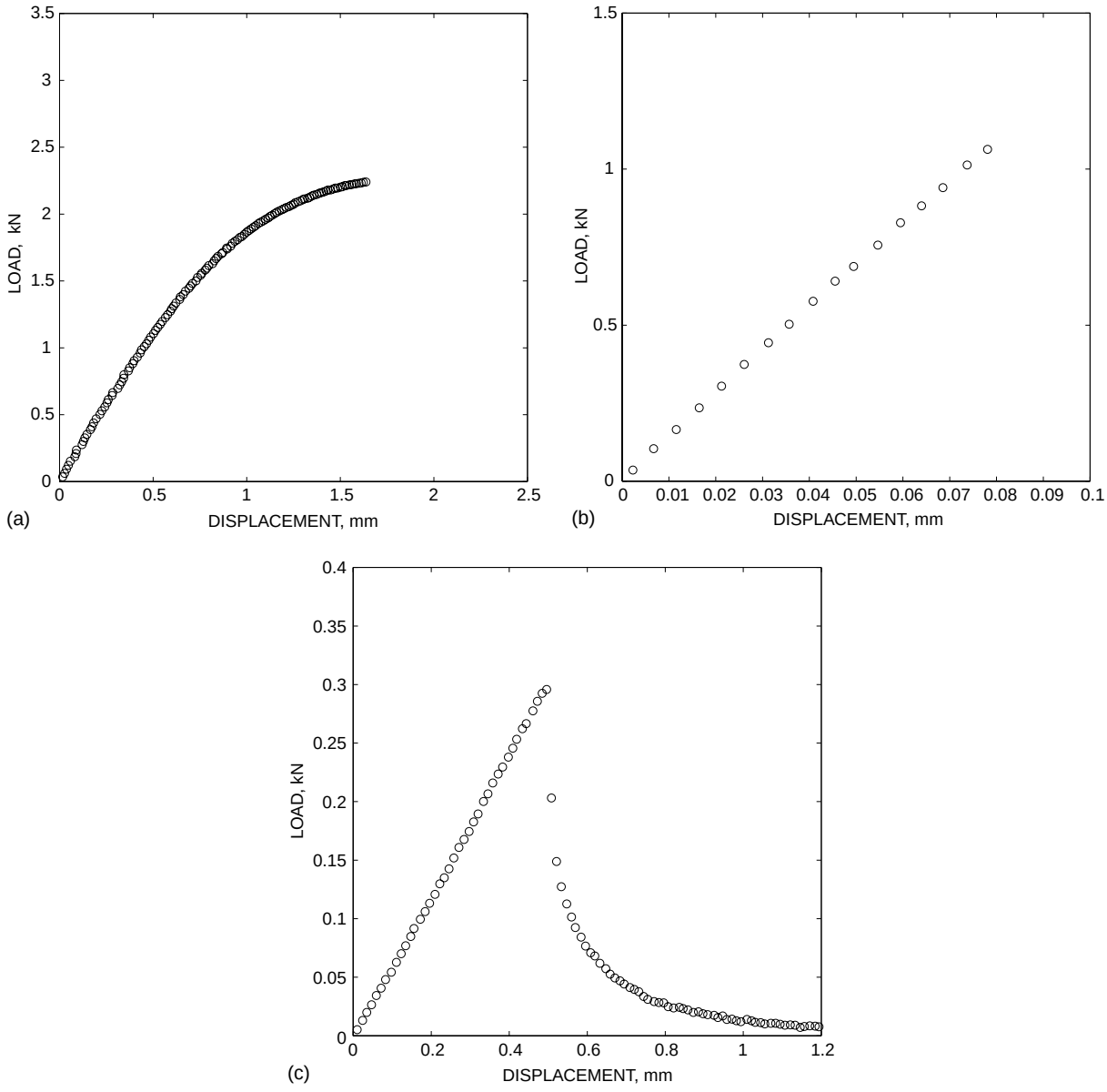

Fig. 3. Experimental load–displacement curves for PMMA: (a) smooth-bar tension; (b) notched-bar tension; and (c) ASTM standard compact tension specimen (without a sharp fatigue pre-crack).

The fit is also shown in Fig. 4. We caution that the values of craze-initiation parameters are expected to be quite sensitive to the quality of the machined surfaces, and also to the grade of the material from which the specimens are made. We also recognize that three data points are perhaps not quite enough to unambiguously specify the non-linear dependence of $\sigma_{1,\mathrm{cr}}$ on σ. However, the trend of a decreasing value of $\sigma_{1,\mathrm{cr}}$, with an increasing value of the mean normal stress σ, is clearly revealed by the data. Information from more

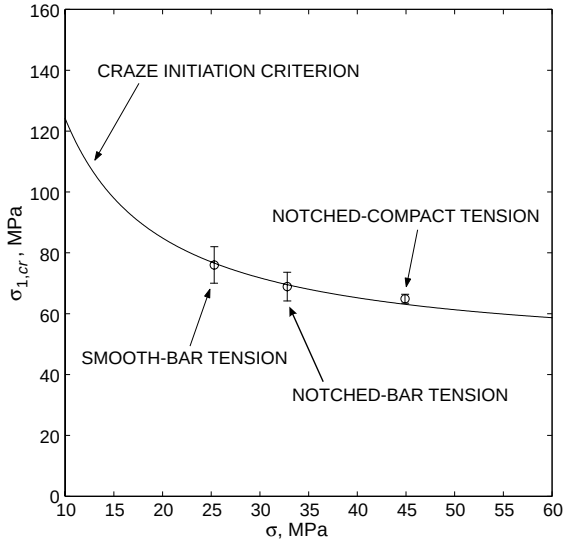

Fig. 4. Fit of the craze-initiation criterion to the experimental data from smooth-bar, notched-bar, and notched compact tension specimens.

complete experimental programs, as it becomes available, can easily be incorporated into our constitutive framework and numerical capability for modeling crazing.

Step 2. Recall that we have assumed that the strain-rate sensitivity parameter for craze widening is taken to be the same as that for shear-flow, $m = 0.043$, and that the reference craze strain rate ξ_0 is set by enforcing the continuity of the plastic stretching in switching from shear-flow to craze-flow, Eq. (3.1). The craze-flow resistance parameter s_{craze} is estimated from the stress levels observed in a simple compression experiment at a large value of compression. From Fig. 2 we estimate that

$$s_{\text{craze}} = 200 \text{ MPa}.$$

Step 3. The craze-breakdown parameter, $\epsilon_{\text{f}}^{\text{p}}$, is estimated by repeating the numerical calculations for the three sets of experiments, using both the shear-flow and the craze-initiation and craze-flow parameters estimated above, and adjusting the value of $\epsilon_{\text{f}}^{\text{p}}$ to match the failure portion of the load–displacement curves. Since craze-breakdown and fracture occur rather abruptly in the smooth-bar and notched-bar tension experiments, the value of $\epsilon_{\text{f}}^{\text{p}}$ is best estimated from the notched compact-tension specimens because of the stable crack propagation observed in these experiments. A value of

$$\epsilon_{\text{f}}^{\text{p}} = 0.005$$

provides the best calibration to the load–displacement curves from the compact tension specimens. [17]

[17] In a remarkable set of experiments on specimens with near perfect surfaces and no trapped foreign particles (made from fibers drawn from individual polystyrene pellets), Argon and Hannoosh (1977) found that their PS specimens showed macroscopic inelastic deformation with a ductility of 5–8% (their Fig. 6). The macroscopic inelastic deformation was a result of extensive closely-spaced crazes ($\approx$10 μm apart) which produced whitening of the gauge section. Post-mortem microscopic examination revealed that the crazes were $\approx$0.5 μm wide. Based on a craze-width at craze-fracture of $\approx$0.5 μm, and a craze spacing of $\approx$10 μm, one obtains a macroscopic craze strain of $\approx$5%, as observed by Argon and Hannoosh (1977). The smaller value of $\epsilon_{\text{f}}^{\text{p}} = 0.5\%$ observed in our experiments is directly attributable to the imperfections and surface roughness effects in our macroscopic less well-controlled experiments.

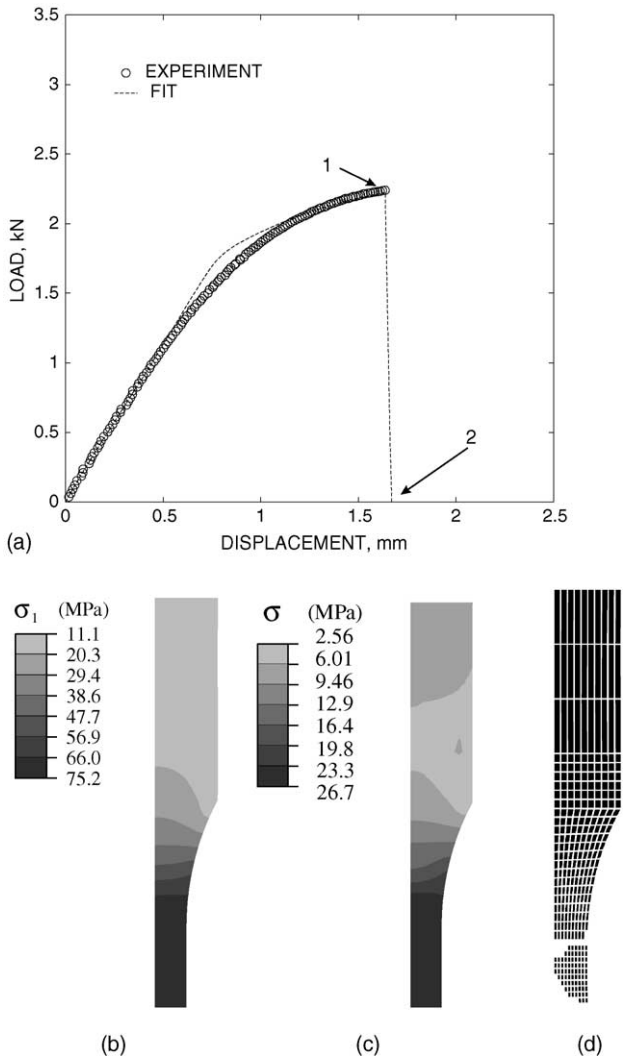

Fig. 5. (a) Experimental and calculated load–displacement curves for a smooth-bar tension specimen. (b) Contours of σ_1, and (c) σ at incipient craze-flow, location 1; (d) mesh at location 2 showing fracture. Note that fracture has occurred at multiple locations in the gauge section.

Using the material parameters for shear-flow, together with those for craze-initiation, flow and breakdown estimated above, Fig. 5 shows the measured and numerically-calculated load–displacement curves for a smooth-bar tension experiment. The load–displacement response is well captured by the model. *Note that the initial break in the numerical load–displacement curve is because of the onset of shear-flow, which precedes the craze-flow and fracture in PMMA*. Contour plots of the maximum principal stress σ_1, and the mean normal stress σ at a location just prior to peak load, are shown in Fig. 5b and c, respectively. Once the craze-breakdown conditions are met, the numerical simulation shows fracture at multiple locations, as indicated in the "failed" mesh of Fig. 5d. This numerical result is consistent with the experimental observation that smooth-bar tension specimens fracture at multiple locations in the gauge section.

Fig. 6a shows the measured and numerically-calculated load–displacement curves for a notched-bar tension experiment. Contour plots of σ_1 and σ at locations 1 and 2 on the numerical curve of Fig. 6a are

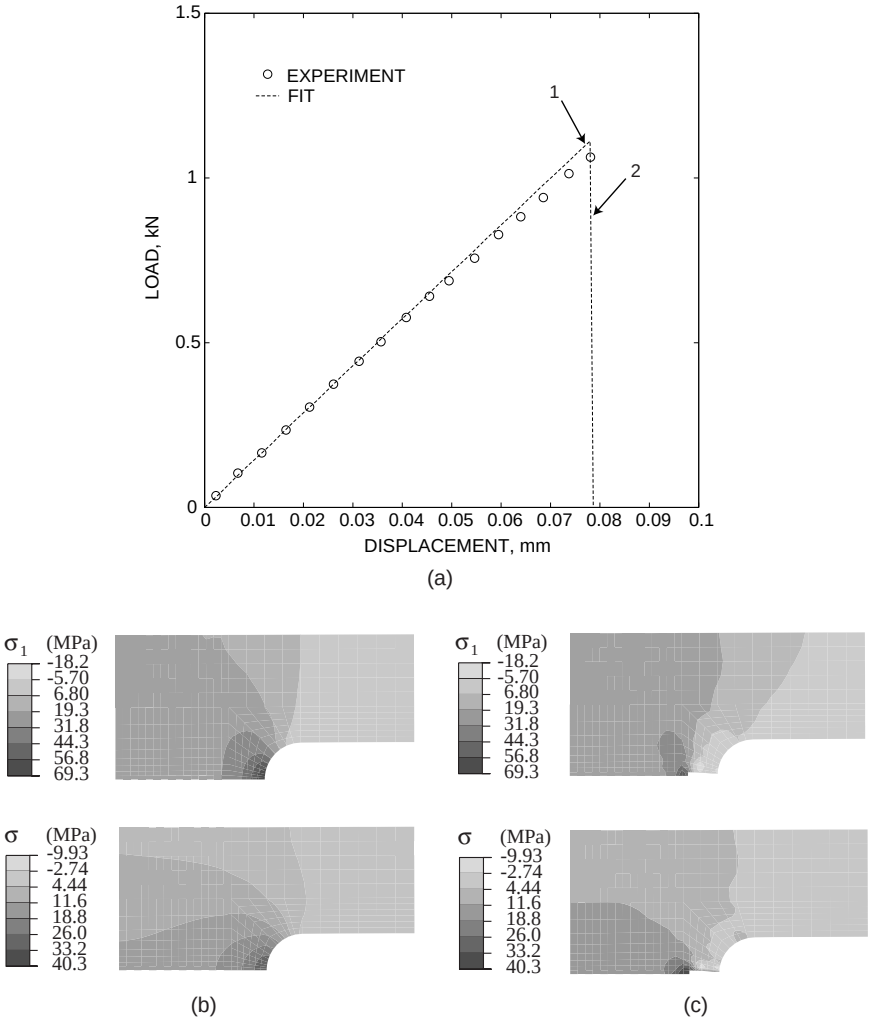

Fig. 6. (a) Experimental and calculated load–displacement curves for a notched-bar tension specimen. (b) Contours of σ_1 and σ at incipient craze-flow, location 1 marked in (a). (c) Contours of σ_1 and σ after craze-fracture has propagated part of the way into the cross-section, location 2 marked in (a).

shown in Fig. 6b and c. The contours in Fig. 6b indicate that crazing initiates at the notch-root. Fig. 6c shows that the craze front and the crack due to craze-breakdown propagate into the specimen in a direction perpendicular to the applied tensile load on the notched specimen.

Fig. 7a shows the measured and numerically-calculated load–displacement curves for an experiment on a compact tension specimen. Contour plots of σ_1, σ, and ϵ^p at locations 1 and 2 on the numerical curve of Fig. 7a are shown in Fig. 7b and c, respectively. The contours in Fig. 7b indicate that crazing initiates at the notch-root, and those in Fig. 7c show that the craze front and the crack due to craze-breakdown propagate into the specimen in a direction perpendicular to the applied tensile load on the notched compact tension specimen. Note that fracture (as modeled by the element-removal technique) is confined to the elements adjacent to the symmetry plane of the simulation, and the contours of the craze strain ϵ^p in Fig. 7c show

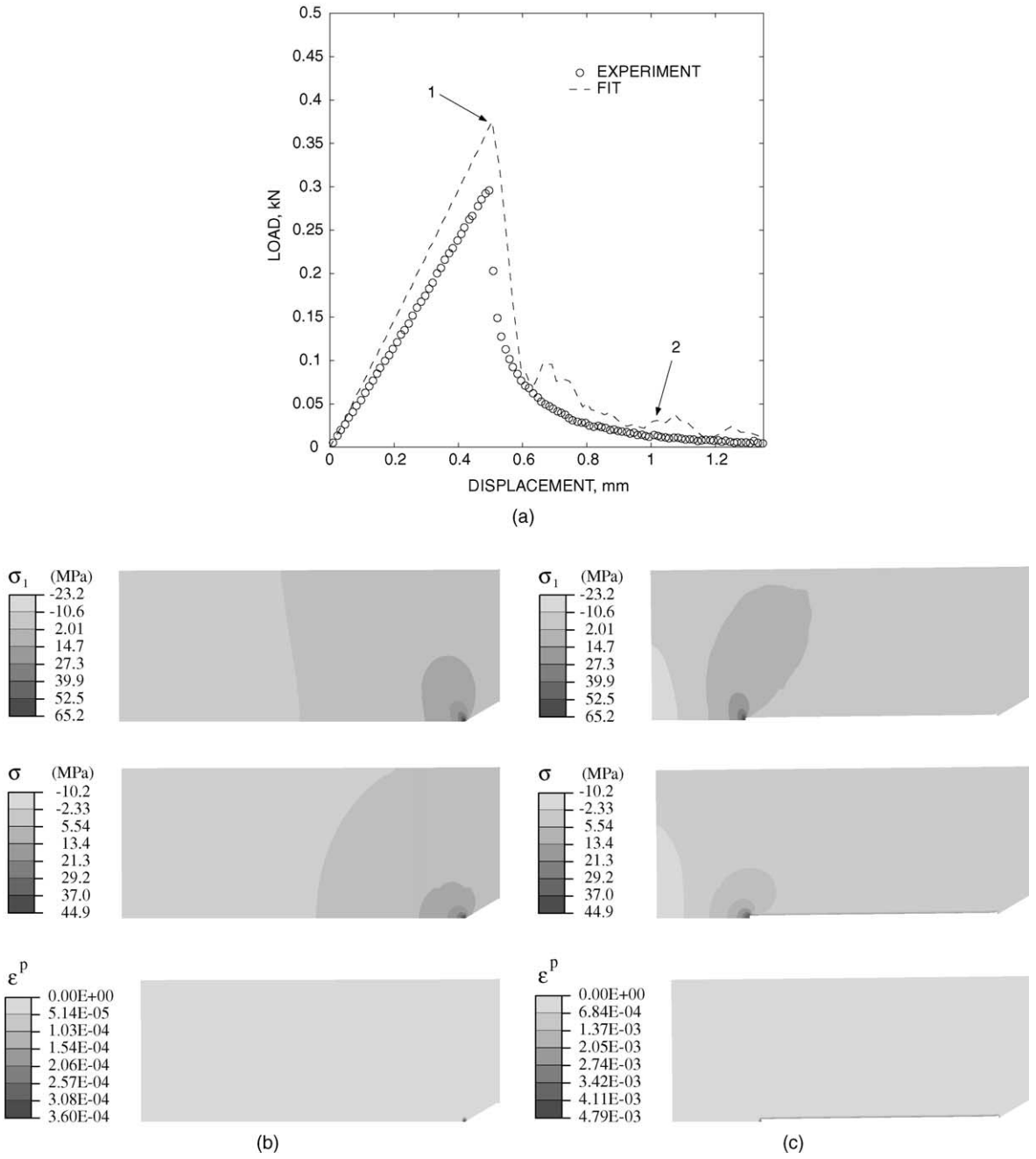

Fig. 7. (a) Experimental and calculated load–displacement curves for a notched compact tension specimen. (b) Contours of σ_1, σ, and ϵ^p at incipient craze-flow, location 1 marked in (a). (c) Contours of σ_1, σ, and ϵ^p after craze-fracture has propagated part of the way into the cross-section, location 2 marked in (a). For clarity of presentation, the contour plots are focused on the region in the vicinity of the notch-root.

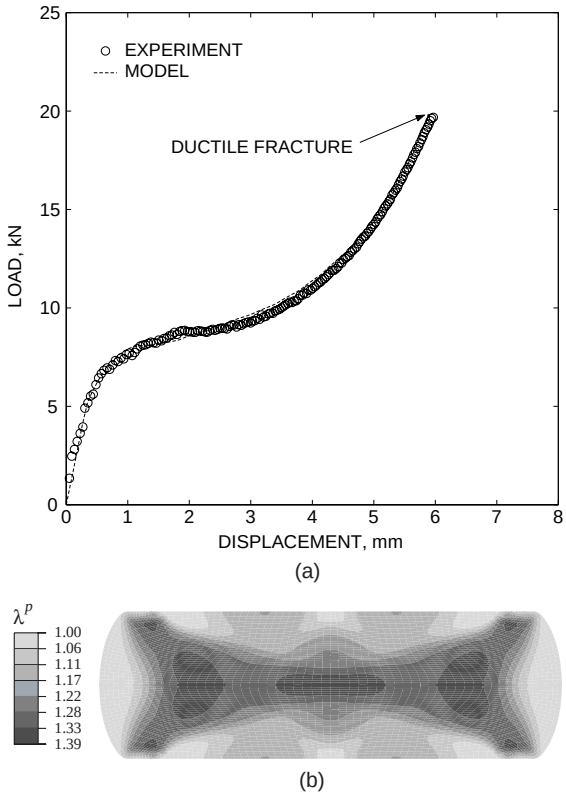

Fig. 8. Fit of the ductile failure criterion in plane strain compression: (a) Load–displacement curve. (b) Contour plot showing values of λ^{p} at the point of ductile fracture.

that, while the elements adjacent to the traction-free crack face have suffered some craze-flow, they have not failed due to craze-breakdown.

Finally, in order to obtain the material parameter $\lambda_{\mathrm{f}}^{\mathrm{p}}$ for ductile fracture, results from a plane strain compression experiment were utilized. In such an experiment crazing and craze fracture are inhibited, but ductile fracture in the material can still occur by the chain-scission mechanism at large values of λ^{p}. The full specimen geometry is modeled using a fine mesh of 3900 ABAQUS/CPE4R plane strain elements. The compression platens are modeled using rigid surfaces, and a coefficient of friction of 0.08 is assumed to model the interface friction between the lubricated PMMA and tool steel surfaces. The measured and calculated load–displacement curves [18] are shown in Fig. 8; the point of ductile fracture initiation is also indicated. A contour plot of λ^{p} at ductile fracture initiation is shown in Fig. 8b; this yields a value of

$$\lambda_{\mathrm{f}}^{\mathrm{p}} = 1.390$$

for the initiation of ductile fracture.

[18] The experimental load–displacement curve has been corrected for machine and punch/die compliances.

4. Investigation of predictive capabilities of the model

In this section we investigate the accuracy of the numerical predictions from our calibrated model for PMMA. We study the deformation and fracture of two prototypical notched components: (a) a thin plate with a circular hole loaded in tension; and (b) a notched beam loaded in four-point bending.

4.1. Tension of a thin plate with a circular hole

The specimen geometry for this experiment is shown in Fig. 9a. The full three-dimensional geometry is modeled using 26,084 ABAQUS/C3D8R elements; a detail of the fine mesh in the vicinity of the hole is shown in Fig. 9b. Fig. 9c shows that the numerically-predicted load–displacement curve is in very good agreement with the one that was experimentally-measured. *Note that the load–displacement curve is non-linear, once again showing evidence of some shear-flow prior to crazing.* The specimen fractured at a displacement of about 1.4 mm into multiple pieces, and showed extensive crack-branching prior to final failure, Fig. 10a. [19] A corresponding image from the numerical simulation is shown in Fig. 10b.

Fig. 11 shows contour plots of σ_1 and σ at three instances keyed to the numerical load–displacement curve in Fig. 9c. At location 1, Fig. 11a, the stress distribution shows that a maximum value of $\sigma_1 = 74.7$ MPa and $\sigma = 26.8$ MPa occur at opposite edges of the hole. Since at $\sigma = 26.8$ MPa, the critical value of σ_1 is $\sigma_{1,\mathrm{cr}} = 74.9$ MPa, the stress state at location 1 is just before that necessary to satisfy the craze-initiation criterion. By location 2, Fig. 11b, craze-flow and fracture have occurred at opposite edges of the hole, as indicated by the removed elements. [20] At this location, the fracture process is seen to be symmetric about the window. However, by location 3, Fig. 11c, the cracks have branched away from the centerline of the specimen; this occurs because of small local numerical perturbations.

The numerical simulation nicely captures the major features observed in the physical experiment: (a) the non-linear load–displacement curve, (b) the process of crack initiation and propagation with crack-branching, and (c) fracture into multiple pieces.

4.2. Bending of a notched beam

Four-point bending experiments were conducted on notched specimens, whose geometry is shown schematically in Fig. 12a. As indicated in this figure, specimens with a notch of 1.98 mm root radius were tested. A specimen width of 50 mm was chosen so as to approximate plane strain conditions at the notch-root. The experiments were performed by displacing the center rollers relative to the outer rollers at a constant displacement rate of 2 mm/min. All rollers were constrained during the experiments to ensure that they did not rotate. To simulate bending of the sharp-notched beam, one-half of the beam is modelled using 1370 ABAQUS/CPE4R plane strain elements. A detail of the finite-element mesh at the notch-root is shown in Fig. 12b.

Fig. 13a compares the experimentally-measured and numerically-predicted load–displacement response. [21] This time the numerical curve under-predicts the load at fracture by about 20%. The reasons for this under-prediction are not known, but the fact that the actual loads are higher, indicates that crazing in the four-point notch-bend experiment initiates at higher levels of σ_1 and σ than those predicted by curve-fit

[19] Four different experiments were conducted, and the overall response from the different experiments was very similar, with the displacements at which fracture occurred varying by less than 4%.

[20] Recall that we are using an element-removal technique to model fracture propagation.

[21] The load–displacement curve from the experiment has been corrected for an estimated compliance of 0.57 mm/kN of loading system.

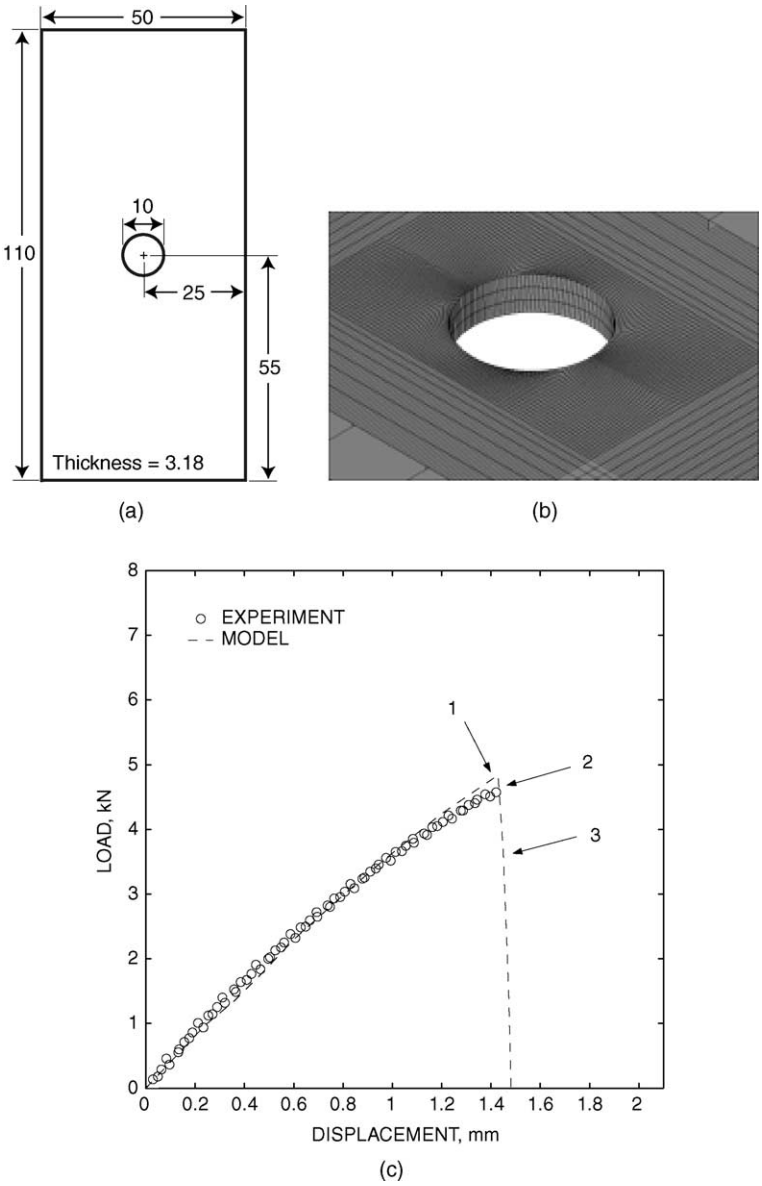

Fig. 9. (a) Specimen geometry with dimensions in mm. (b) Detail of the finite-element mesh in the vicinity of the hole. (c) Comparison of the experimentally-measured and numerically-predicted load–displacement curves.

for craze-initiation in PMMA, shown in Fig. 4. We attribute the major reason for this discrepancy to the sensitivity of the craze-initiation criterion to various statistical effects such as material variability and surface finish that we have not fully-explored in our work. Fig. 13b and c show the contours of σ_1 and σ at initiation of craze-flow, and also once the crack has propagated along the specimen centerline, well into the beam. Cracking due to crazing initiates at the notch-root, and propagates into the beam along the specimen centerline. We note that although the numerical simulation under-predicts the load at failure, it nicely captures the process of crack nucleation and propagation due to crazing.

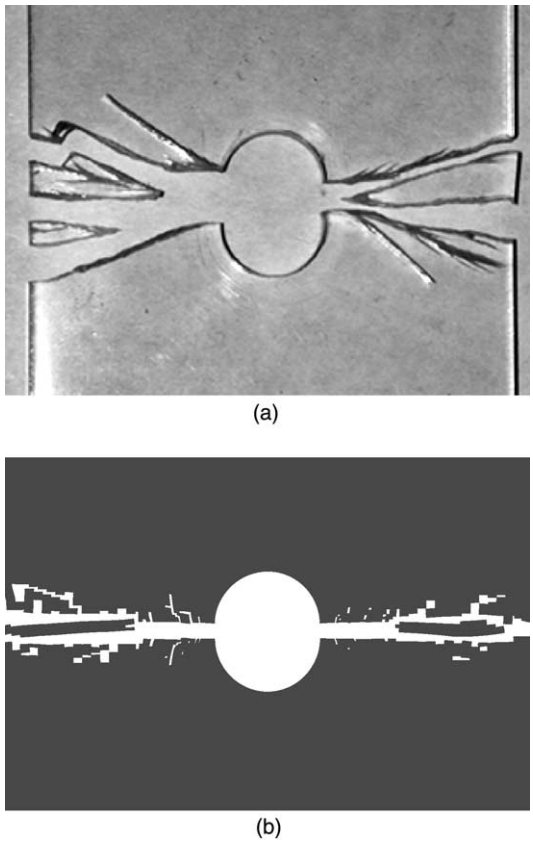

Fig. 10. (a) Image of fractured specimen showing crack-branching and fractured ligaments. Loading direction is vertical. (b) Result from corresponding numerical calculation.

5. Concluding remarks

Most previous models for fracture of glassy polymers have been based on the standard framework of linear elastic fracture mechanics. This approach ignores the important details of the process of crazing in flexible chain glassy polymers, and it cannot be used when shear-yielding of the material may be occurring at other locations in the body, especially when there are no initial sharp cracks in the body. Although the phenomenon of crazing has been widely studied over the past four decades, and considerable understanding of the micromechanisms of crazing and cracking in amorphous polymers has been developed, the incorporation of this understanding into an engineering tool for the quantitative prediction of the deformation and fracture response of glassy polymers is just beginning to emerge. Of particular note is the recent work of Van der Giessen and co-workers (Estevez et al., 2000; Tijssens et al., 2000a,b), based on "cohesive surface" modeling of crazing. These authors used an elastic–viscoplastic traction-separation relation which accounts for the three separate stages of craze-initiation, widening, and breakdown. While they have produced informative two-dimensional numerical simulations, much work remains to be done to correlate their parametric studies with actual experimental results. Here, instead of attempting to represent each individual craze with an interface element, we have developed a continuum-level model which contains the three ingredients of crazing, viz., initiation, widening, and breakdown. We have allowed for local inelastic deformation due to shear-yielding in possible concurrence with that due to crazing, and introduced a

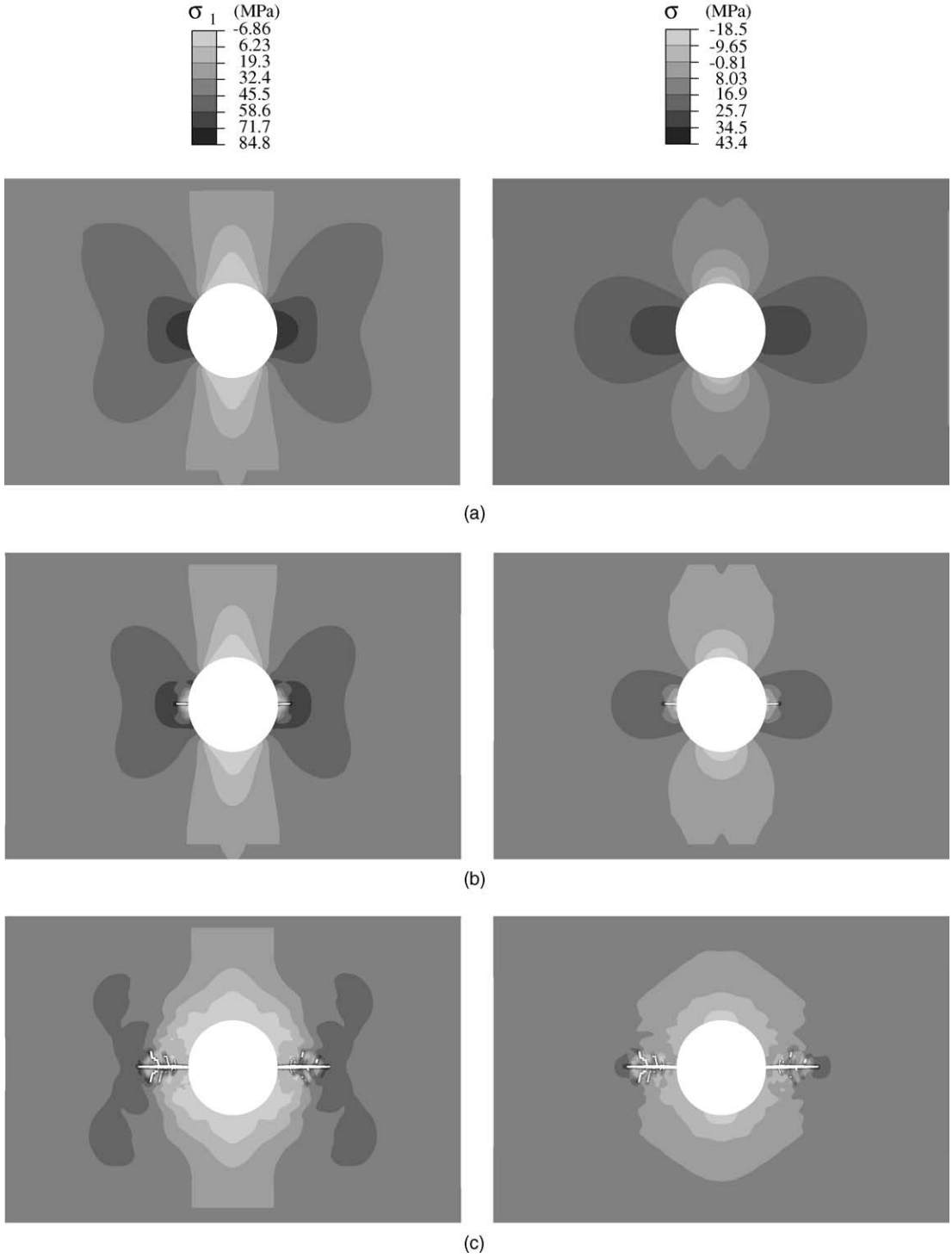

Fig. 11. Contour plots of σ_1 and σ at (a) location 1, (b) location 2, and (c) location 3 indicated on the numerical load–displacement curve in Fig. 9. Loading direction is vertical.

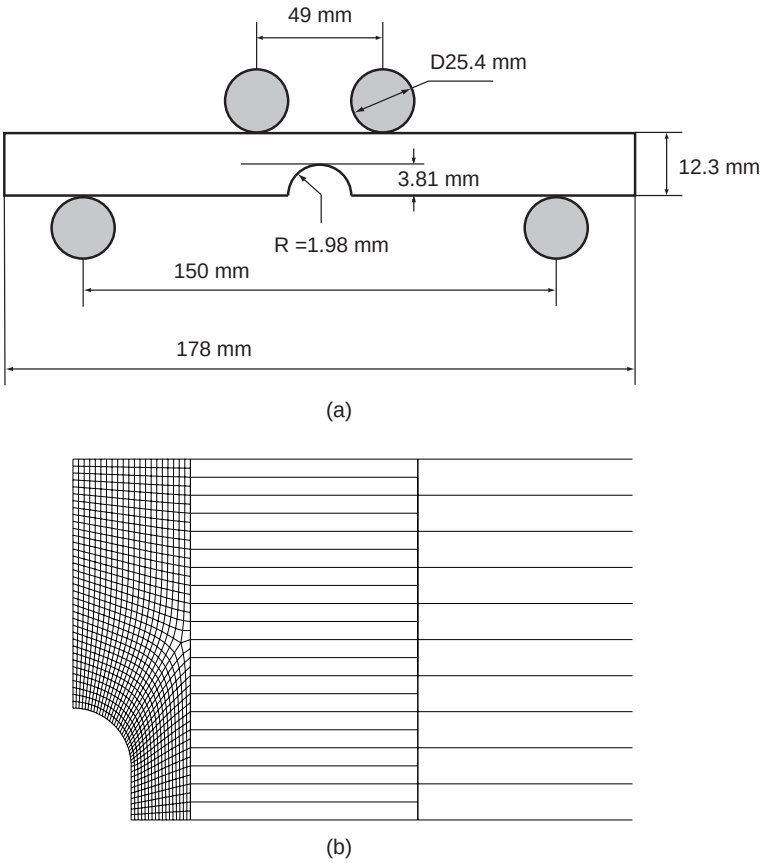

Fig. 12. (a) Schematic geometry (not to scale) of four-point bending experiment. The specimen has a nominal width of 50 mm. (b) Detail of finite-element mesh at the notch-root.

craze-initiation criterion based on the local maximum principal tensile stress reaching a critical value which depends on the local mean normal stress. After crazing has initiated, our continuum model represents the transition from shear-flow to craze-flow by a change in the viscoplastic flow rule, in which the dilational inelastic deformation associated with craze-plasticity is taken to occur in the direction of the local maximum principal stress. Finally, for situations in which the local maximum tensile stress is positive, craze-breakdown and fracture is taken to occur when a local tensile plastic craze strain reaches a critical value. We have implemented our constitutive model in a finite-element computer program. We have calibrated the constitutive parameters in our model for PMMA, and shown that our model, when suitably calibrated and implemented, is able to reasonably-well predict the macroscopic load–displacement curves, and local aspects of the craze-flow and fracture processes in two prototypical notched components made from this material. [22]

In summary, we have attempted to develop the framework of an engineering tool for the quantitative prediction of the deformation and fracture response of glassy polymers. The results presented here

[22] We recognize that, as with all finite-element calculations, our numerical modeling of the craze-fracture process may be "mesh-sensitive". We have not conducted exhaustive "mesh-sensitivity" analyses for the numerical results presented in this paper. Much needs to be done to refine the meshes (amongst other considerations) to be able to better represent such fracture processes. However, we consider that the proposed constitutive model, failure criteria, together with the element-removal methodology, numerically-capture the highly non-linear complex fracture processes in polymers, in a reasonably-acceptable fashion (for a first attempt).

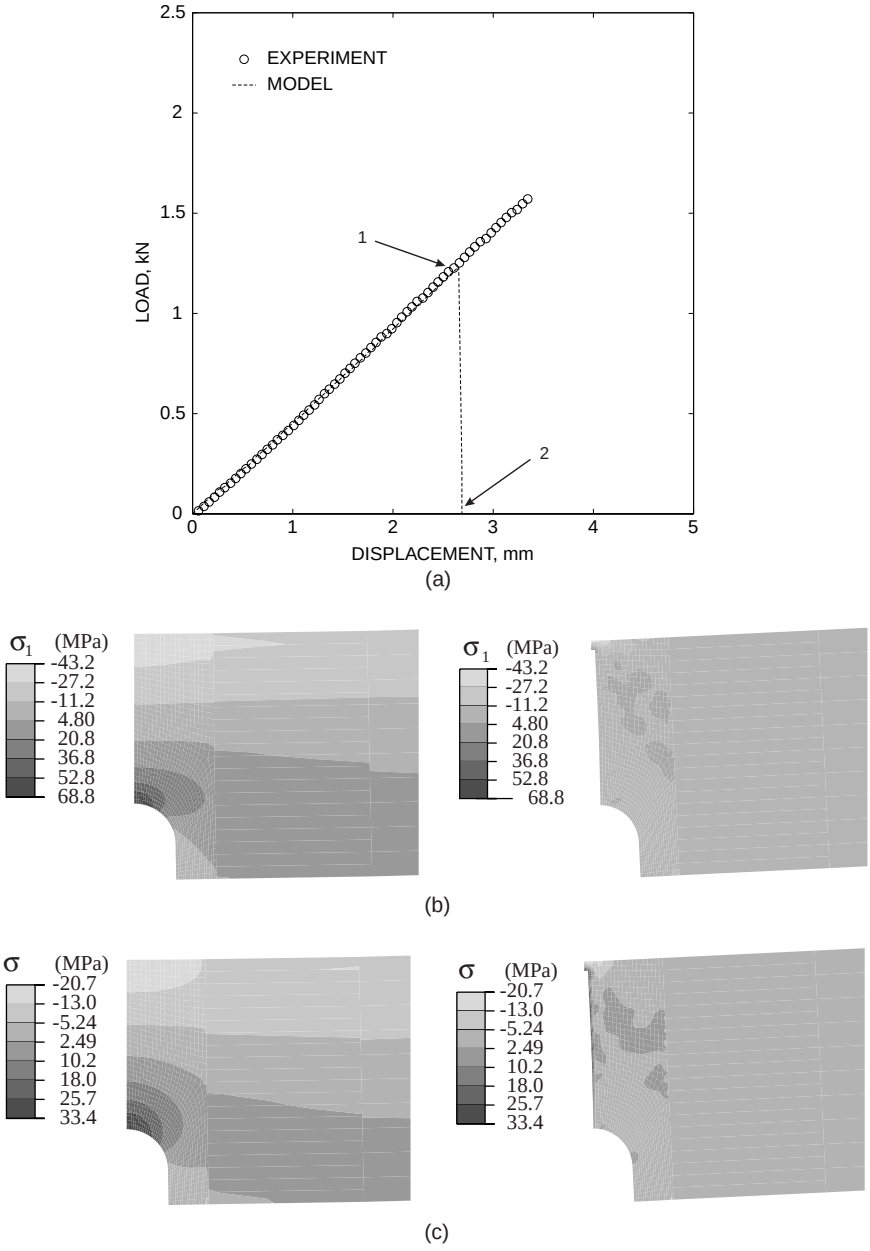

Fig. 13. Four-point bending of a sharp-notched beam: (a) comparison of the numerical load–displacement response against the experiment. Contour plots of σ_1 and σ at (b) location 1, and (c) location 2. Brittle fracture occurs along the specimen centerline.

represent a first step towards this goal. Much additional work needs to be performed for this framework to be more-fully fleshed out, and to be truly predictive. Some issues that need special further attention are (i) *craze-initiation*: The central ingredient in the continuum model for crazing is the craze-initiation criterion. It is well known that because of the importance of imperfections in controlling the local stress states and the

sites of craze-initiation, stress-based criteria for craze-initiation are hard to determine with precision from experiments. Thus, much work needs to be done to elucidate the statistical aspects of craze-initiation (and also craze-breakdown). (ii) *Effects of strain rate, temperature and the environment*: The present research needs to be extended by conducting additional experiments at various strain-rates and temperatures. Further, we have limited our attention to normal dry conditions. It is well known that crazing is very sensitive to the environment, the effects of which need to be appropriately accounted for.

Acknowledgements

Financial support provided by the Singapore-MIT Alliance is gratefully acknowledged. LA acknowledges valuable discussions with Ali Argon on various aspects of the inelastic deformation and fracture of amorphous polymers. The ABAQUS finite-element code was made available under an academic license to MIT from HKS, Inc., Pawtucket, RI.

References

ABAQUS, 2002. Reference manuals. Hibbit, Karlsson & Sorenson, Inc., Pawtucket, RI.

Anand, L., 1996. A constitutive model for compressible elastomeric solids. Computational Mechanics 18, 339–352.

Anand, L., Gurtin, M.E., 2003. A theory of amorphous solids undergoing large deformations, with application to polymeric and metallic glasses. International Journal of Solids and Structures 40, 1465–1487.

Andrews, E.H., 1973. Cracking and crazing in polymeric glasses. In: Haward, R.N. (Ed.), The Physics of Glassy Polymers, first ed. Applied Science, pp. 394–453.

Argon, A.S., 1999. Craze plasticity in low molecular weight diluent-toughened polystyrene. Journal of Applied Polymer Science 72, 13–33.

Argon, A.S., Hannoosh, J.G., 1977. Initiation of crazes in polystyrene. Philosophical Magazine 36, 1195–1216.

Argon, A.S., Hanoosh, J.G., Salama, M.M., 1977. Initiation and growth of crazes in glassy polymers. Fracture 1, 445–470.

Arruda, E.M., Boyce, M.C., 1993. Evolution of plastic anisotropy in amorphous polymers during finite straining. International Journal of Plasticity 9, 697–720.

Barenblatt, G.I., 1959. The formation of equilibrium cracks during brittle fracture: general ideas and hypotheses, axially symmetric cracks. Applied Mathematics and Mechanics (PMM) 23, 622–636.

Boyce, M.C., Parks, D.M., Argon, A.S., 1988. Large inelastic deformation of glassy polymers, part 1: Rate dependent constitutive model. Mechanics of Materials 7, 15–33.

Camacho, G.T., Ortiz, M., 1996. Computational modeling of impact damage in brittle materials. International Journal of Solids and Structures 33, 2899–2938.

Donald, A.M., 1997. Crazing. In: Haward, R.N., Young, R.J. (Eds.), The Physics of Glassy Polymers, second ed. Chapman & Hall, pp. 295–341.

Dugdale, D.S., 1960. Yielding of steel sheets containing slits. Journal of the Mechanics and Physics of Solids 8, 100–104.

Estevez, R., Tijssens, M.G.A., Van der Giessen, E., 2000. Modeling of the competition between shear yielding and crazing in glassy polymers. Journal of the Mechanics and Physics of Solids 48, 2585–2617.

Kambour, R.P., 1973. A review of crazing and fracture in thermoplastics. Journal of Polymer Science 7, 1–154.

Kinloch, A.J., Young, R.J., 1983. Fracture behavior of polymers. Elsevier.

Kramer, H.H., 1983. Microscopic and molecular fundamentals of crazing. Advances in Polymer Science 52, 1–56.

Kroner, E., 1960. Allgemeine kontinuumstheorie der versetzungen und eigenspannungen. Archive for Rational Mechanics and Analysis 4, 273–334.

Lee, E.H., 1969. Elastic plastic deformation at finite strain. ASME Journal of Applied Mechanics 36, 1–6.

Narisawa, I., Yee, A.F., 1993. Crazing and fracture of polymers. Materials Science and Technology. A Comprehensive Treatment 12, 699–765.

Oxborough, R.J., Bowden, P.B., 1973. A general critical-strain criterion for crazing in amorphous polymers. Philosophical Magazine 28, 547–559.

Parks, D.M., Argon, A.S., Bagepalli, B., 1985. Large elastic–plastic deformation of glassy polymers. Part 1: Constitutive modeling. MIT, Program in Polymer Science and Technology Report.

Rabinowitz, S., Ward, I.M., Parry, J.C., 1970. The effect of hydrostatic pressure on the shear yield behavior of polymers. Journal of Materials Science 5, 29–39.

Socrate, S., Boyce, M.C., Lazzeri, A., 2001. A micromechanical model for multiple crazing in high-impact polystyrene. Mechanics of Materials 33, 155–175.

Sternstein, S.S., Meyers, F.A., 1973. Yielding of glassy polymers in the second quadrant of principal stress space. Journal of Macromolecular Science Physics B 8, 539–571.

Sternstein, S.S., Ongchin, L., 1969. Yield criteria for plastic deformation of glassy high polymers in general stress fields. Polymer Preprints 10, 1117–1124.

Tijssens, M.G.A., Van der Giessen, E., Sluys, L.J., 2000a. Modeling of crazing using a cohesive surface methodology. Mechanics of Materials 32, 19–35.

Tijssens, M.G.A., Van der Giessen, E., Sluys, L.J., 2000b. Simulation of Mode I crack growth in polymers by crazing. International Journal of Solids and Structures 37, 7307–7327.

Treloar, L.R.G., 1975. The Physics of Rubber Elasticity. Oxford.

Williams, J.G., 1984. Fracture Mechanics of Polymers. Ellis Horwood.

Wu, P.D., Van der Giessen, E., 1993. On improved network models for rubber elasticity and their applications to orientation hardening of glassy polymers. Journal of the Mechanics and Physics of Solids 41, 427–456.

Xu, X.P., Needleman, A., 1994. Numerical simulations of fast crack growth in brittle solids. Journal of the Mechanics and Physics of Solids 42, 1397–1434.